

PAPER • OPEN ACCESS

Deformation behaviour of aluminium nanocrystals under shock-wave loading

To cite this article: A M Vlasova 2019 *J. Phys.: Conf. Ser.* **1385** 012049

View the [article online](#) for updates and enhancements.



IOP | ebooks™

Bringing together innovative digital publishing with leading authors from the global scientific community.

Start exploring the collection—download the first chapter of every title for free.

Deformation behaviour of aluminium nanocrystals under shock-wave loading

A M Vlasova^{1,2}

¹ Institute of Metal Physics of the Ural Branch of the Russian Academy of Sciences, Sofya Kovalevskaya Street 18, Ekaterinburg, 620219, Russia

² Ural Federal University, Lenina Avenue 51, Ekaterinburg, 620000, Russia

E-mail: alisa-12005@yandex.ru

Abstract. Nonequilibrium process of shock-wave loading of aluminum nanocrystals were investigated numerically under uniaxial stress conditions using molecular dynamics simulations (MD). Deformation curves, time dependence of strain rate and the change in potential energy were constructed. Calculated properties of aluminium using embedded atom interatomic potential are compared with each other. Relationship between the calculated characteristics are discussed. The behaviour of deformation curves for two different aluminium nanocrystals is explained. The problems of modeling the deformation hardening of aluminum nanocrystals are considered.

1. Introduction

Shock compression of condensed matter occurs in a wide variety of situations, including high-speed automobile and aircraft collisions, explosive welding, armor penetration, meteor impacts, interstellar dust-dust collisions and inertial confinement fusion. The strain rate in experiment can reach 10^6 s^{-1} [1, 2].

The loading process is usually short-pulse. The processes of formation of crystal structure defects, nucleation, growth of dislocations and twins [3], redistribution and output of dislocations on the free surface take place in several picosecond. Aluminium is a metal with a face-centered cubic crystal lattice and its nanocrystals of different orientations have different deformation ability. A detailed consideration of the features of the deformation behavior of nickel (FCC) in the simulation by molecular dynamics calculations is given in the paper [4]. Aluminum has a higher stacking faults defects energy (250 mJ/m^2) than nickel (150 mJ/m^2). Due to periodic boundary conditions in the work [4] mainly stacking faults defects observed, which are rarely observed experimentally. Experimental and theoretical studies of different types of dislocation slip conclude that the main type of sliding in aluminium is octahedral slip [5]. The behaviour of aluminium nanocrystal under impact loading conditions and especially the shock wave propagation are still not well understood. The shock wave propagation through the nanocrystal material structure under impact loading conditions has a significant effect on its deformation mechanism and therefore it is imperative to understand its effects thoroughly. Strain curves for shock-wave loading cannot be obtained experimentally. Molecular dynamics is a method that allows to model processes at small characteristic times. The purpose of this study is the molecular dynamic simulation of compression of defectless nanosized aluminium single



crystal, the computation of strain, strain rates, and potential energy curves under shock-wave loading. [001] and [11 $\bar{1}$] aluminium nanocrystals were selected to compare the results.

2. Setup of MD simulation

The MD simulations are performed using the code large-scale atomic molecular massively parallel simulator (LAMMPS) [6] in dynamic loading conditions together with the embedded atom method (EAM) potential [7]. The calculated data were processed with the Open Visualization Tools OVITO [8]. Table 1 compares physical properties of aluminium predicted by the Mendelev with experimental data, where C_{11} , C_{12} , C_{44} are elastic modulus.

Table 1. Physical properties of aluminium (target value and calculated by the Mendelev [9] potentials)

Properties	C_{11} , GPa	C_{12} , GPa	C_{44} , GPa
Expt.	107.30	60.08	28.3
Mendelev	101.53	64.50	36.67

The simulated cluster is an face-centered cubic lattice of the aluminium in the form of a rectangular parallelepiped of size $20.2 \times 20.2 \times 28.3$ nm and $11.4 \times 19.8 \times 38.4$ nm with the edges of the crystallographic orthogonal directions $x = [100]$, $y = [010]$, $z = [001]$ and $x = [\bar{1}21]$, $y = [101]$, $z = [11\bar{1}]$ for [001]- and [11 $\bar{1}$]-nanocrystal respectively. The boundary conditions in the directions x , y , z was set as free and shrink-wrapped. Simulated dislocations could emerge on the surface. Deformation was implemented by redetermining the velocities of the atoms located in the surface end layers with a thickness of 0.6 nm, which made in sum about 5% of the distance along the crystallographic axis of loading. The thickness of the surface layer was chosen empirically (proceeding from the optimal calculation time). Along the Z axis of the laboratory coordinate system, the velocity projections for the atoms in loaded layers were fixed, whereas no limitations were imposed on the velocities of atoms in other crystallographic directions. The moduli of velocities corresponded to the value $V = 4$ m/s, and the directions in different layers were oriented towards the center of the modeled system. In the directions of the X and Y axes of the laboratory coordinate system, the velocity projections for the atoms in the end layers were zero. The system temperature was 300–500 K. Mechanical work was performed on the system and the total energy of the system was not saved. A symmetric stress tensor σ_{IJ} , stored as a 6-element vector is computed by the formula

$$\sigma_{IJ} = \frac{\sum_k^N m_k \cdot v_{kI} \cdot v_{kJ}}{V} + \frac{\sum_k^{N'} r_{kI} \cdot f_{kJ}}{V}, \quad (1)$$

where $N = N'$ is the number of atoms in the system (nonperiodic boundary conditions), V is the system volume, r_I , f_I and m_I are the position, force vector and mass, I and J are x , y , z . The 6 components of the vector are ordered xx , yy , zz , xy , xz , yz . The first term uses components of the kinetic energy tensor and the second term uses components of the virial tensor. Strain ε was calculated as

$$\varepsilon = \frac{\Delta L_n}{L_0}, \quad (2)$$

where ΔL_n is linear shortening of the aluminium nanocrystal in the loading direction, L_0 – initial length of the aluminium nanocrystal in the loading direction. Deformation curves was plotted as stress vs strain with a time step of 0.001 ps.

3. Stress-strain curve

“Stress σ/σ_{\max} – strain ε ” curves for aluminium nanocrystals were calculated. Figure 1 shows stress σ/σ_{\max} as a function of strain ε for aluminium [001] and $[11\bar{1}]$ -nanocrystals deformed at $2 \times 10^8 \text{ s}^{-1}$ initial strain rate. Both curves monotonically increase to $\varepsilon = 0.04$ – 0.05 , then a sharp break occurs and the curve goes to the plateau. Several quantitative characteristics in the description of the deformation curves are offered. Maximum stress σ_{\max} is associated with the homogeneous origin of dislocations. $\sigma_{\max}^{[001]} = 43 \text{ GPa}$, $\sigma_{\max}^{[11\bar{1}]} = 67 \text{ GPa}$. Minimum stress σ_{\min} shows the applied stress to start the plastic flow. $\Delta\varepsilon$ is width of the transition from homogeneous dislocation nucleation to nonhomogeneous motion and multiplication of dislocations. $\sigma_{\max}/\sigma_{\min}$ characterizes the stress level of homogeneous nucleation in comparison with the applied stress of plastic flow. Thus, the introduced characteristics reflect the strength and plastic properties of the simulated material. These characteristics are entered as quantitative values to compare strength and plastic properties of different nanocrystal under high-speed loading. Modeling and calculation are the only ways to obtain deformation curves for high-speed loading. The above characteristics are determined from the deformation curves. As can be seen in figure 1 the curves are identical. Linear growth to the maximum value of stress σ_{\max} is replaced by a sharp decline to the minimum value of stress σ_{\min} . Further the stress reaches a plateau. Stresses of developed deformation for [001] and $[11\bar{1}]$ aluminium nanocrystals are $0.25\sigma_{\max}$. The linear section of elastic deformation is accompanied by a sawtooth modulation of the straight line. Sawtooth is expressed more clearly for [001] orientation. For hexagonal metals, the calculated deformation curves are given in [10].

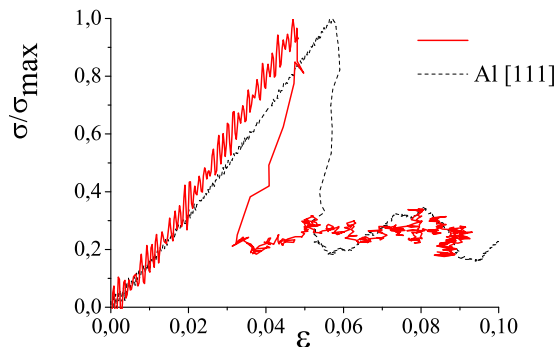


Figure 1. Stress σ/σ_{\max} vs strain ε for aluminium [001]-nanocrystal (red solid line) and $[11\bar{1}]$ -nanocrystal (black dotted line)

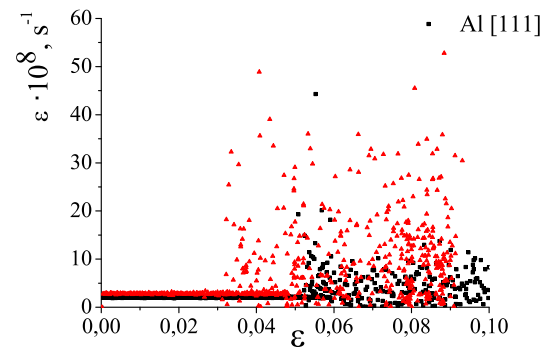


Figure 2. Modulus of strain rate $\dot{\varepsilon}$ vs strain ε for [001]-nanocrystal (red triangular) and $[11\bar{1}]$ -nanocrystal (black rectangle)

4. Strain rate

Figure 2 shows the change in the modulus of strain rate in the deformation process. In the elastic region, the deformation rate is constant regardless of the orientation and is equal to $2.5 \times 10^8 \text{ s}^{-1}$. However, with the advent of dislocations and the development of plastic deformation, the situation changes. For [001] orientation the rate module changes in the interval $(2.5\text{--}55.0) \times 10^8 \text{ s}^{-1}$, the average module exceeds the initial rate 10 times. For $[11\bar{1}]$ orientation the rate module changes in the interval $(2.5\text{--}35.0) \times 10^8 \text{ s}^{-1}$, the average module exceeds the initial rate one by 5 times. The strain rate bursts are associated with overcoming dislocations barriers and depends on the barrier energy. The abrupt nature of the strain rate in the plastic region is evidence of the heterogeneity of the deformation process.

5. Potential energy

Molecular dynamics is used to study the nonequilibrium process of high strain-rate shock-wave loading [9]. Since the system is being worked on, the total energy of the system E_{tot} is not saved. The change of potential energy of systems in the process of deformation is shown in figure 3. It may be noted that the curve repeats the strain curve. Monotonic growth in the elastic region is replaced by a sharp decline. However, as the strain ε increases, the potential energy E_{pot} of the system increases too. The curve has a pronounced sawtooth character for [001] orientation. The transition from the elastic to the plastic region has a stroke anomaly. The nonmonotonic curves immediately after the origin of dislocations is due to the achievement of a high level of shear stresses. Dislocations are accelerated to high speeds and the rate of plastic deformation becomes much higher than the external deformation. Therefore, the strain rate at some points in time may be negative.

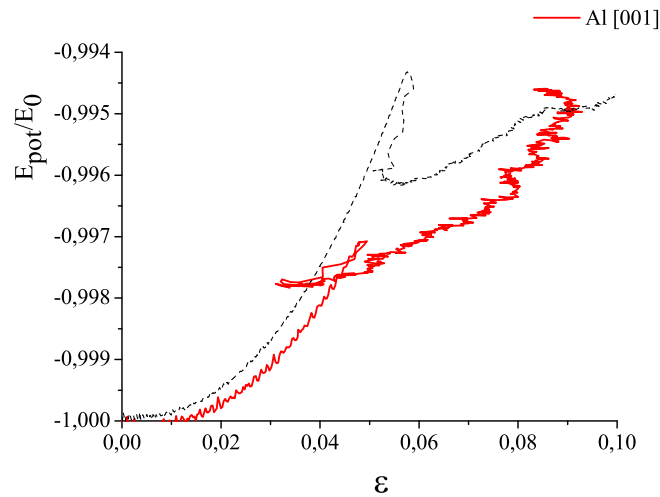


Figure 3. Potential energy E_{pot}/E_0 vs strain ε for aluminium [001]-nanocrystal (red solid line) and [111]-nanocrystal (black dotted line)

6. Microstructure

It was said above about the stress of homogeneous nucleation of dislocations. Evidence of this is the presence of dislocation loops at strain ε less than 0.04–0.05. Figure 4 shows a loop consisting of screw and edge segments, the burgers vector is $b = 1/6 \langle 112 \rangle$ ($\varepsilon = 0.04$, [001]-monocrystal). Due to the presence of free surfaces, the origin of dislocations from the surface cannot be excluded.

It is shown (figure 5) the change of microstructure for the two considered orientations of nanocrystals of aluminum. There are traces of dislocations on the surface (figure 4(a), (b), (d), (e)) which are of the same type for both orientations. [001] nanocrystals are characterized by a greater number of dislocation segments in the volume of the simulated cell. The figure 4(c) shows the number of segments after 600 ps from the beginning of calculation ($\varepsilon = 9.7\%$). Edge segments (green curves) with low mobility are predominant. The dislocation structure of [111]-nanocrystal after 600 ps ($\varepsilon = 11\%$) from the beginning of the calculation is shown in figure 4(f). It can be seen that the edge segments are much smaller than in figure 4(c). In both cases, the dislocations have $1/6 \langle 112 \rangle$ and $1/2 \langle 110 \rangle$ Burgers vector.

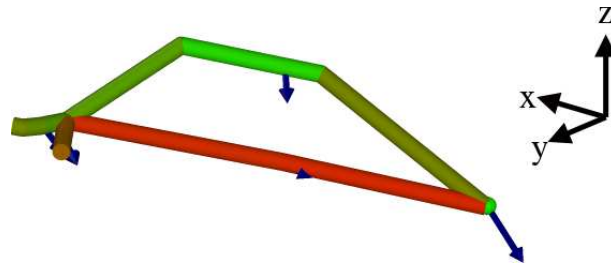


Figure 4. Dislocation loop for aluminium [001]-nanocrystal ($\varepsilon = 0.04$). Red line – screw character, green line – edge character of dislocations, blue arrow – Burgers vector

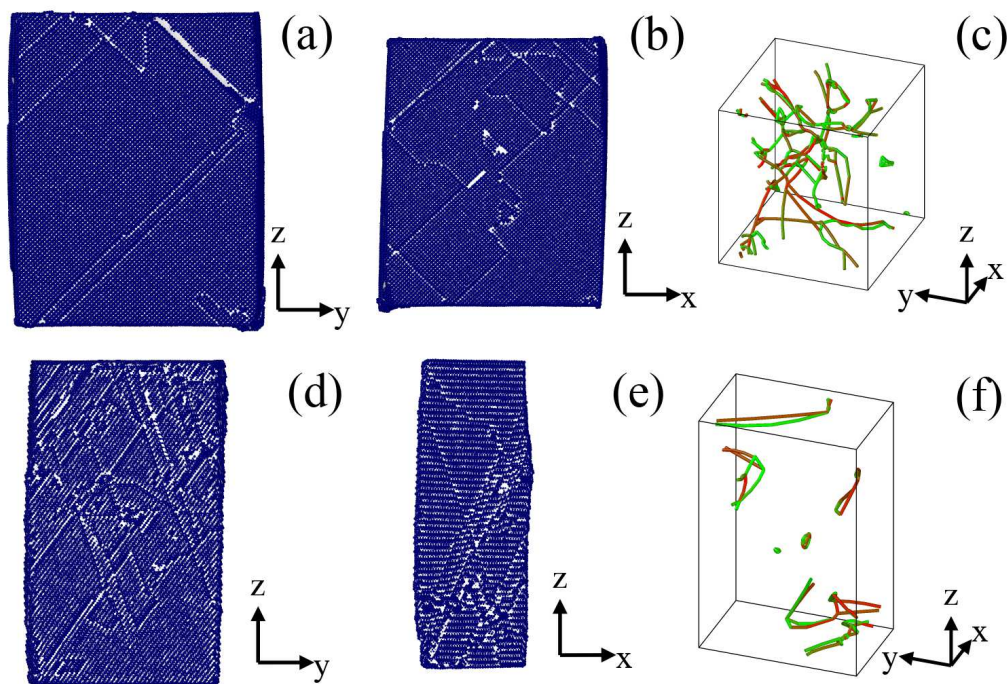


Figure 5. Changing the simulated cell for aluminium [001]-nanocrystal (*a-c*) and $[11\bar{1}]$ -nanocrystal (*d-f*). (*a*), (*b*), (*d*), (*e*) – slip lines, (*c*), (*f*) – dislocation structure (600 ps). Red line – screw character, green line – edge character of dislocations

Stacking faults defects in cubic crystals are a thin layer of the hexagonal phase (HCP) [11]. As a result of the structural analysis (OVITO) it was revealed that for both orientations the content of HCP did not exceed 0.2%.

7. Conclusion

Molecular-dynamic model of high strain-rate shock-wave loading of aluminum nanocrystals was constructed. As based on the idea of the atomic structure of matter, taking into account only the forces of interaction between atoms, which have a quantum-mechanical character to describe massive bodies. Precise calculation of the change in the strain rate over time allows us to judge the heterogeneity of the process. Plastic deformation of the metal is heterogeneous at the micro level. There are a number of different related processes which are closely related

to deformation. At the macro level, deformation is a form change, as at the atomic level, it is the evolution of point, linear and surface defects of the crystal structure. Any polycrystalline and monocrystalline material is deformed inhomogeneously. In addition, different single crystals have different deformation ability. Crystals with a face-centered cubic lattice are plastic enough. However, $[11\bar{1}]$ -orientation is considerably hardened in the process of deformation. The average stress value of the plateau region for both orientations is $\sigma/\sigma_{\max} = 0.25$ (figure 1). Since $\sigma_{\max}^{[001]} < \sigma_{\max}^{[11\bar{1}]}$, the developed plastic deformation for orientation $[001]$ occurs at stresses almost 1.5 times lower than for $[11\bar{1}]$. This is due to the multiple sliding and the formation of dislocation barriers, which is confirmed experimentally. However, over time, thermal fluctuation processes can break down dislocation barriers, softening the material. A recrystallized structure is observed experimentally in a solid after severed deformation. In the process of shock-wave loading relaxation processes in the solid are suppressed. Modeling of high strain-rate process allows us to understand the feature of crystallite deformation. According to Schmid's law, there are six active sliding systems for $[001]$ single crystal and two active systems for $[11\bar{1}]$ single crystal. Multiple sliding generates dislocation barriers, dislocations "get stuck" in the material, hardening is observed. $[001]$ nanocrystall demonstrates the sawtooth shape in the plastic region, the deviation from the average strain rate of 10–20 times, and the sawtooth shape of the potential energy E_{pot} curve. This indicates a considerable heterogeneity of deformation for a given orientation. The sawtooth character of the curve in the elastic region is associated with the instability of the system, and is probably due to the high value of C_{11} . Nanocrystallite $[11\bar{1}]$ shows a smooth shape of the stress-strain and potential energy curves, the deviation from the average strain rate of 5–10 times.

Acknowledgments

The research was carried out within the state assignment of FASO of Russia (theme "Pressure" No. AAAA-A18-118020190104-3). The results of the work have been obtained using Uran supercomputer of IMM Ural Branch of Russian Academy of Science.

References

- [1] Kanel G I *et al* 2007 *Uspekhi Fiz. Nauk.* **177** 809–830
- [2] Bringa E *et al* 2006 *Nature Mater.* **5** 805–809
- [3] Vlasova A M and Nikonov A Y 2018 *Crystallogr. Rep.* **63** 331–338
- [4] Jarmacani H N *et al* 2008 *Acta Mater.* **56** 5584–5604
- [5] Demir E 2017 *Modelling Simul. Mater. Sci. Eng.* **25** 1–23
- [6] Plimpton S 1995 *J. Comp. Phys.* **117** 1–9
- [7] Mendelev M I, Kramer M J, Becker C A and Asta M 2008 *Phil. Mag.* **88**(12) 1723–1750
- [8] Stukowski A *et al* 2010 *Modelling Simul. Mater. Sci. Eng.* **18** 015012
- [9] Kiselev S P 2014 *J. Appl. Mech. Tech. Phys.* **55** 470–493
- [10] Rawat S and Mitra N 2018 *Comp. Mat. Sci.* **141** 19–29
- [11] Hirth J and Lothe J 1982 *Theory of Dislocations* (Criegee Publishing Company)